Passively *Q*-switched ytterbium-doped fiber laser using the evanescent field interaction with bulk-like WTe_2 particles

Seunghwan Ko (高承煥), Jinho Lee (李珍昊), and Ju Han Lee (李周翰)*

School of Electrical and Computer Engineering, University of Seoul, Seoul 02504, Republic of Korea
**Corresponding author: j.h.lee@ ieee.org*

Received October 23, 2017; accepted November 10, 2017; posted online January 26, 2018

The potential of bulk-like WTe_2 particles for the realization of a passive *Q*-switch operating at the 1 μm wavelength was investigated. The WTe_2 particles were prepared using a simple mechanical exfoliation method together with Scotch tape. By attaching bulk-like WTe_2 particles, which remained on the top of the sticky surface of a small segment of the Scotch tape, to the flat side of a side-polished fiber, a saturable absorber (SA) was readily implemented. A strong saturable absorption was then readily obtained through an evanescent field interaction with the WTe_2 particles. The modulation depth of the prepared SA was measured as ~2.18% at 1.03 μm. By incorporating the proposed SA into an all-fiberized ytterbium-doped fiber ring cavity, stable *Q*-switched pulses were readily achieved.

OCIS codes: 140.3510, 140.3540, 160.4330.
doi: 10.3788/COL201816.020017.

Q-switched fiber lasers have been useful light sources for many applications, such as material processing, light detection and ranging (LIDAR), laser surgery, and supercontinuum generation[1–4]. Since *Q*-switched pulses are generated by either a passive or an active switching of the laser oscillator *Q*-factor, the temporal width of their output pulses usually ranges from nanoseconds to microseconds. Compared with mode-locking, *Q*-switching can be easily induced in a fiberized resonator, since it does not require a careful design of the cavity–fiber parameters for the achievement of a balance between the dispersion and nonlinearity.

For the implementation of passively *Q*-switched fiber lasers, saturable absorbers (SAs) are commonly used to induce the *Q*-factor modulation within their cavities. Although semiconductor-based SAs have been widely used in practice as a passive *Q*-switch[5], a range of their drawbacks, such as the need of complicated fabrication-facility processes and a limited operational wavelength, motivated a number of researchers throughout the world to investigate low-cost and effective-performance alternative SA materials, including carbon nanotubes (CNTs)[6,7], graphene[8,9], black phosphorus[10–13], topological insulators[14–17], transition-metal dichalcogenides (TMDs)[18–31], filled skutterudites[32], and MXene[33].

Recently, TMDs have attracted great technical attention in the photonic and electronic fields, since their bandgap structures can be engineered by controlling the number of the bandgap layers[34]. TMDs are composed of a hexagonal layer of metal atoms (M) that are sandwiched between two chalcogen-atom (X) layers with a common formula of MX_2. The binding of the TMD monolayers by weak van der Waals forces produces a bulk structure. These materials possess excellent optoelectronic properties, such as a large saturable absorption, strong Kerr nonlinearity, and possible valley polarization, which are useful for the device implementation in the fields of plasmonics, quantum electrodynamics, and ultrafast photonics[35–38].

Among molybdenum disulfide (MoS_2), tungsten disulfide (WS_2), molybdenum diselenide ($MoSe_2$), molybdenum ditelluride ($MoTe_2$), tungsten diselenide (WSe_2), and tungsten ditelluride (WTe_2), MoS_2 and WS_2 are the TMDs that have been most widely investigated as alternatives to graphene[39,40]. It is well-known that the TMD bandgap varies depending on the number of layers due to the hybridization between the *d* orbitals of the transition-metal atoms and the p_z orbitals of the chalcogen atoms[41], unlike the zero bandgap of graphene. Such a bandgap-engineering property allows for the implementation of a variety of photonic devices, such as optical switches, photo detectors, and quantum-well modulators[38,42].

Recently, the saturable-absorption properties of TMDs have been intensively investigated, and a number of TMD-based SAs have been successfully demonstrated for the implementation of pulsed lasers[18–31]. One of the interesting findings of those investigations is that the TMDs exhibited saturable-absorption properties at the near- and mid-infrared wavelengths even though the upper-cutoff wavelengths that are determined by their bandgap energies are usually below the wavelength of 1 μm. The reason for this abnormal saturable-absorption phenomenon is attributable to a sub-bandgap absorption, which is caused by defects and edge states[43–46]. Furthermore, the authors recently theoretically and experimentally verified that the structural dimensionality of TMDs is not critical regarding their saturable-absorption applications[31]. It was demonstrated that the bulk-like WTe_2 microflake is a low-cost saturable-absorption material that can be readily used for the implementation of broadband SAs.

In this work, the potential of the bulk-like WTe_2 particles for the realization of a passive Q-switch that can be operated at the 1 μm wavelength was further investigated. In particular, a mechanical exfoliation method was used to obtain the bulk-like WTe_2 particles, unlike the authors' previous demonstration, in which a liquid exfoliation method was employed with the use of Scotch tape and without centrifugation[30,31]. The mechanical exfoliation method has been known to be a simple and low-cost technique for the fabrication of the highly crystalline thin nanosheets of layered materials. Since Novoselov *et al.* used the mechanical exfoliation method to obtain graphene layers in 2004[47], it has been widely used for the fabrication of thin layers of other two-dimensional materials for SAs, such as graphene[48], topological insulators[15], and black phosphorus[12]. However, there has been no report on the use of the mechanical exfoliation method for the fabrication of TMD-based SAs to the best of the authors' knowledge.

First, a passive Q-switch was implemented on a side-polished fiber platform. Bulk-like WTe_2 particles that had adhered to a segment of the Scotch tape were then directly placed onto the flat surface of the side-polished fiber without the use of index-matching oil. Due to the residual adhesive on the surface of the Scotch tape, the bulk-like WTe_2 particles were tightly fixed on the flat surface of the side-polished fiber. To check the SA's operability as a passive Q-switch at the 1 μm wavelength, the prepared SA was incorporated into an ytterbium-doped-fiber (YDF)-based ring cavity. Q-switched output pulses were then readily achieved using the laser. By varying the pump power, the repetition rate and the temporal width of the pulses are tunable from ~19.08 to ~79.16 kHz and from ~1 to ~1.69 μs, respectively. So far, quite a few SAs that are based on TMD-deposited side-polished fibers have been demonstrated[23,24,27,30,31]; however, the use of a bulk-like TMD-deposited side-polished fiber for the Q-switching of a 1 μm fiber laser has not been reported.

Figure 1 shows the photo and schematics of our prepared WTe_2-particle-attached side-polished fiber. The side-polished fiber in this experiment was prepared using the commercially available SMF-28 single-mode fiber (Corning, U.S.A.). First, on a V-grooved quartz block, a single-mode fiber was fixed, and its cladding was elaborately polished. The preparation of a fiber-optic device based on the evanescent-field interaction at the 1 μm wavelength is not straightforward, since the evanescent field becomes weaker within the cladding at shorter beam wavelengths[49]. Note that the evanescent field interaction at the 1 μm wavelength is much weaker than that at the 1.55 and 2 μm wavelengths under the same polishing-depth condition. In empirical terms, the optimum distance between the polished surfaces of the optical fiber and the top side of the fiber core for the proposed device is approximately 5 μm, regarding both the proper evanescent field interaction and a reasonable insertion loss. At a wavelength of 1.06 μm, the insertion loss (beam propagation loss) and the polarization-dependent loss (PDL) of the WTe_2-particle-attached side-polished fiber were measured as ~8 dB and ~0.3 dB, respectively. The insertion loss of the WTe_2-particle-attached side-polished fiber is much larger than that of the WTe_2/PVA-film-deposited side-polished fiber at a wavelength of 1.55 μm, as demonstrated in Ref. [31], and this is due to a smaller residual cladding. It should be noted that a further reduction of the distance between the flat surface of the fiber and the top side of the fiber core is impossible due to a significant increase of the beam-propagation loss.

Figure 2(a) shows the measured scanning-electron-microscope (SEM) image of the WTe_2 particles on the top of the sticky surface of the Scotch-tape segment. It is obvious that micrometer-sized, bulk-like particles are randomly distributed together with nanometer-sized particles over the surface.

Raman-spectrum measurements of the WTe_2 particles on the top of the sticky surface of the Scotch-tape segment were then conducted. The measured results on Point A, Point B, and the sticky surface of a small segment of the Scotch tape are shown in Fig. 2(b). At Point A, four typical Raman optical-phonon peaks were observed in the bulk WTe_2, which are A_2^4 at 110 cm^{-1}, A_1^8 at 131 cm^{-1}, A_1^5

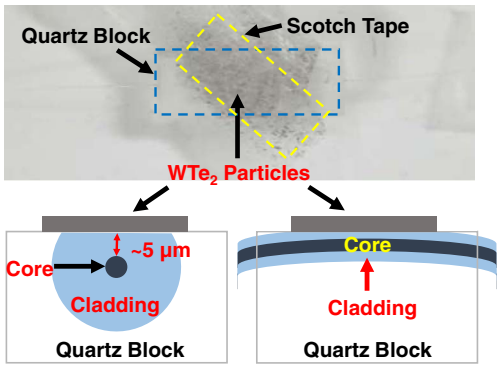

Fig. 1. Photo and schematics of the prepared WTe_2-particle-attached side-polished fiber.

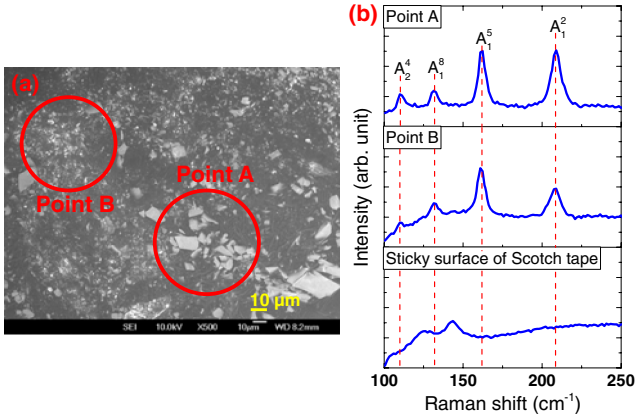

Fig. 2. Measurements of (a) the scanning-electron-microscope (SEM) image and (b) the Raman spectra of the WTe_2 particles on the top of the sticky surface of a small segment of Scotch tape.

at 161 cm^{-1}, and A_1^2 at 208 cm^{-1}. It is well-known that A_2^4 is absent in monolayered WTe_2, while an increase of the number of layers stiffens the A_2^4- and A_1^5-mode frequencies and softens the A_1^8 and A_1^2 modes[50]. On the other hand, in the conventional Raman spectrum of WTe_2, three of the four distinct Raman peaks above 100 cm^{-1} consistently red-shift as the layer number increases up to six. It was reported that WTe_2 with more than six layers exhibits Raman frequencies almost similar to those in bulk WTe_2[51]. As shown in Fig. 2(b), we could find that the frequencies of the Raman spectrum in our prepared WTe_2 particles are almost similar to those in the bulk WTe_2 sample.

Figure 3(a) shows the measured energy-dispersive-spectrometry (EDS) spectrum of the WTe_2 particles on the top of the sticky surface of the Scotch-tape segment. From the EDS spectrum, the atomic tungsten (W) and telluride (Te) contents are ~33.42% and ~66.58%, respectively, indicating that the WTe_2-particle ratio of the W atoms to the Te atoms in the present study is ~1:2, which corresponds to the WTe_2 formula[52].

Then, the nonlinear transmission of the bulk-like WTe_2-particle-attached side-polished fiber was measured in order to calculate its modulation depth and saturation threshold power, as shown in Fig. 3(b). A passively mode-locked YDF laser with a ~2.8 ps pulse width was used at a repetition rate of 37.4 MHz to perform this measurement. The measured data were fitted using a well-known fitting equation[53]. The measured modulation depth is only ~2.18%, and the saturation power is ~1.2 MW. The modulation depth tends to be lower at shorter wavelengths due to a reduced evanescent field interaction[49]. The relatively high nonsaturable loss is due to the large polishing depth and the roughness of the polished surface. It should be noticed that the nonlinear transmission curve in Fig. 3(b) could change, depending on the temporal width of the input pulses[54]. Since a microsecond pulse laser with a high peak power was not available in our laboratory, we used a picosecond mode-locked fiber laser.

Figure 4 shows an experimental schematic of the proposed Q-switched YDF laser with the WTe_2-particle-attached side-polished fiber. The laser was constructed using a simple ring–cavity structure and a 0.8 m length of the SM-YSF-HI YDF (Nufern, U.S.A.), while the gain medium has a peak absorption of ~250 dB/m at 975 nm. Also, the fiberized cavity was pumped by a 975 nm laser diode via a 975/1060 nm wavelength division multiplexer (WDM). For a unidirectional beam oscillation, an optical isolator was inserted. A polarization controller (PC) was then included after the insertion of the isolator due to the optimization of the beam interaction between the WTe_2 particles and the oscillating beam at the surface of the side-polished fiber. The WTe_2-particle-attached side-polished fiber was then inserted between the PC and a coupler as the Q-switch. A 90:10 coupler was used to extract the laser output beam from the ring cavity.

From the fiber–laser setup, Q-switched pulses were achieved at a pump power of ~110 mW. The Q-switched pulses were maintained up to the maximum pump power of 261 mW without any loss of stability. The measured optical spectrum is shown in Fig. 5(a). The central wavelength and the 3 dB bandwidth were measured at ~1044 and ~3.3 nm, respectively. It is well-known that the central wavelength of the output beam from a rare-earth-doped fiber laser is determined depending on the cavity conditions, such as cavity propagation loss, active fiber length, and dopant concentration[55,26]. This is the reason why our laser exhibited the output pulses in the 1040 nm region and not in the 1060 nm region. Figure 5(b) shows the measured oscilloscope traces of the output pulses for various pump powers. The temporal widths of the output pulses were decreased, while the repetition rate was increased as the

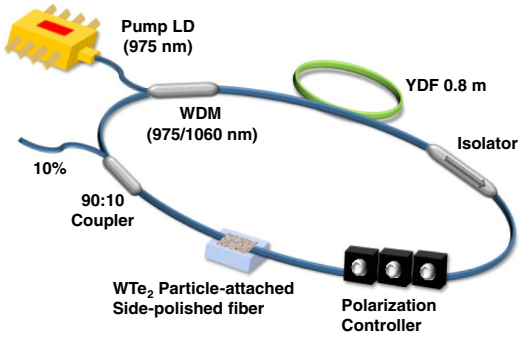

Fig. 4. Experimental configuration of the proposed Q-switched YDF laser.

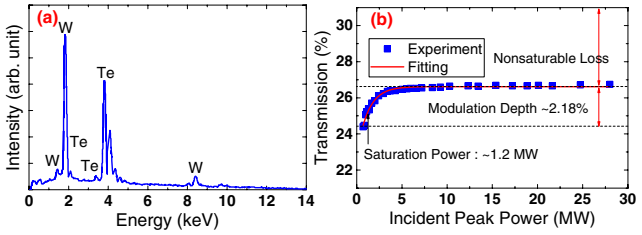

Fig. 3. Measurements of (a) the EDS spectrum of the WTe_2 particles and (b) the nonlinear transmission curve of the WTe_2-particle-attached side-polished fiber.

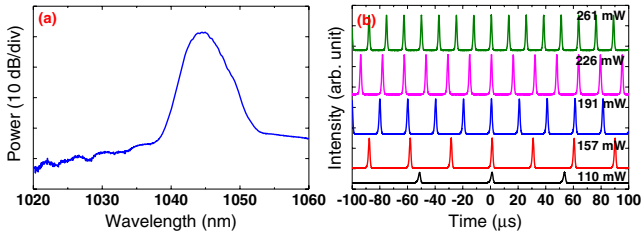

Fig. 5. (a) Measured optical spectrum of the output pulses at a pump power of ~180 mW. (b) Measured oscilloscope traces of the output pulses for various pump powers.

pump power was increased, as is typically expected from passively *Q*-switched fiber lasers[56].

Furthermore, we have conducted an additional experiment without the WTe_2 particles in order to check whether the Scotch tape and its residual glue affect the measurement. When a small segment of Scotch tape with residual adhesive was attached onto the flat side of side-polished fiber, its insertion loss and PDL were measured at ~3.3 and ~0.28 dB, respectively. When it was incorporated into our laser cavity, no *Q*-switching occurred.

Figure 6 summarizes the output pulse characteristic variations, such as the pulse width, repetition rate, energy, and average output power, as functions of the pump power. Figure 6(a) shows the measured *Q*-switched pulse width and repetition rate versus the increased pump power. The repetition rate and the pulse width changed from ~19.08 to ~79.16 kHz and from ~1.69 to ~1 μs, respectively. The sharp decrease of the temporal width of the output pulses at a pump power more than 240 mW is believed to be due to the existence of parasitic continuous waves, which can partially bleach the SA and thus change its saturable-absorption property[29,57,58]. The pulse energy and the average optical power of the output pulses were measured as a function of the input pump power, as shown in Fig. 6(b). The maximum pulse energy and output power are ~28.3 nJ and ~2.2 mW, respectively. It is believed that an optimization of the cavity parameters may improve the output power performance.

Finally, the output performance of the implemented *Q*-switched YDF laser in this study was compared with that of a *Q*-switched YDF laser for which a bulk-structured bismuth telluride (Bi_2Te_3)-topological-insulator-deposited side-polished fiber is used[58], as shown in Table 1. The modulation depth of the proposed bulk-like WTe_2-particle-based SA is slightly smaller than that of the bulk-structured Bi_2Te_3-topological-insulator-based one. The maximum pulse energy and pump efficiency of our *Q*-switched YDF laser are lower than the values of the laser using the bulk-structured Bi_2Te_3-topological-insulator-deposited side-polished fiber. At present, it is unclear whether the performance difference between the two lasers is due to the different material properties or the slightly different laser configurations, so a further investigation needs to be conducted.

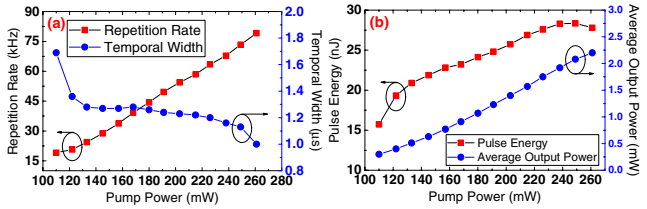

Fig. 6. (a) Measured repetition rates and temporal widths of the *Q*-switched pulses as a function of the pump power. (b) Measured pulse energies and average powers as a function of the pump power.

In conclusion, the use of a 1 μm SA that is based on bulk-like WTe_2 particles for the *Q*-switching of a YDF laser has been successfully demonstrated. The preparation of the WTe_2 particles involved the inclusion of a small segment of Scotch tape in a simple mechanical exfoliation method. By attaching bulk-like WTe_2 particles, which remained on the top of the sticky surface of the small Scotch tape segment, to the flat side of a side-polished fiber, the SA was readily obtained without the use of index-matching oil. Then, its saturable-absorption performance was experimentally verified using both a nonlinear saturable-absorption measurement and a *Q*-switched fiber laser experiment. Interestingly, a strong saturable absorption that is based on the mutual interaction between the bulk-like WTe_2 particles and the propagation beam was readily observed.

This experimental demonstration reaffirms that bulk-like WTe_2 is an effective nonlinear optical material for the implementation of broadband SAs, which is claimed by our previous study in Ref. [31].

This work was supported by the National Research Foundation of Korea funded by the Korean Government (MSIT), South Korea (Grant Nos. NRF- 2015R1A2A2A11000907 and NRF-2015R1A2A2A04006979); Ministry of Science and ICT (MSIT), Korea, under the Information Technology Research Center (ITRC) support program (IITP-2017-2015-0-00385), supervised by the Institute for Information and Communications Technology Promotion (IITP).

Table 1. Performance Comparison of Passively *Q*-switched Ytterbium-doped Fiber Lasers Using a Side-polished Fiber with Saturable-absorption Materials.

Saturable Absorption Materials	Modulation Depth (%)	*Q*-switching Threshold (mW)	Wavelength (nm)	Max. Pulse Energy (nJ)	Repetition Rate (kHz)	Min. Pulse Width (μs)	Max. Output Power (mW)	Pump Efficiency (%)	Refs.
Bulk-structured Bi_2Te_3	2.5	114	1056	38.3	35–77	1	2.95	1.45	[59]
Bulk-like WTe_2	2.18	110	1044	28.3	19–79	1	2.2	0.84	This work

References

1. Z. J. Chen, A. B. Grudinin, J. Porta, and J. D. Minelly, Opt. Lett. **23**, 454 (1998).
2. R. J. De Young and N. P. Barnes, Appl. Opt. **49**, 562 (2010).
3. S. V. Chernikov, Y. Zhu, J. R. Taylor, and V. P. Gapontsev, Opt. Lett. **22**, 298 (1997).
4. A. Y. Chamorovskiy, A. V. Marakulin, A. S. Kurkov, T. Leinonen, and O. G. Okhotnikov, IEEE Photon. J. **4**, 679 (2012).
5. Z. Yu, M. Malmström, O. Tarasenko, W. Margulis, and F. Laurell, Opt. Express **18**, 11052 (2010).
6. S. Y. Set, H. Yaguchi, Y. Tanaka, and M. Jablonski, J. Lightwave Technol. **22**, 51 (2004).
7. D.-P. Zhou, L. Wei, B. Dong, and W.-K. Liu, IEEE Photon. Tech. Lett. **22**, 9 (2010).
8. Q. Bao, H. Zhang, Y. Wang, Z. Ni, Y. Yan, Z. X. Shen, K. P. Loh, and D. Y. Tang, Adv. Funct. Mater. **19**, 3077 (2009).
9. J. Liu, S. Wu, Q.-H. Yang, and P. Wang, Opt. Lett. **36**, 4008 (2011).
10. J. Sotor, G. Sobon, W. Macherzynski, P. Paletko, and K. M. Abramski, Appl. Phys. Lett., **107**, 051108 (2015).
11. S. B. Lu, L. L. Miao, Z. N. Guo, X. Qi, C. J. Zhao, H. Zhang, S. C. Wen, D. Y. Tang, and D. Y. Fan, Opt. Express **23**, 11183 (2015).
12. Y. Chen, G. Jiang, S. Chen, Z. Guo, X. Yu, C. Zhao, H. Zhang, Q. Bao, S. Wen, D. Tang, and D. Fan, Opt. Express **23**, 12823 (2015).
13. K. Park, J. Lee, Y. T. Lee, W.-K. Choi, J. H. Lee, and Y.-W. Song, Ann. der Phys. **527**, 770 (2015).
14. C. Zhao, H. Zhang, X. Qi, Y. Chen, Z. Wang, S. Wen, and D. Tang, Appl. Phys. Lett. **101**, 211106 (2012).
15. J. Sotor, G. Sobon, W. Macherzynski, P. Paletko, K. Grodecki, and K. M. Abramski, Opt. Mater. Express **4**, 1 (2014).
16. Y. Chen, C. Zhao, S. Chen, J. Du, P. Tang, G. Jiang, H. Zhang, S. Wen, and D. Tang, IEEE J. Sel. Top. Quantum Electron. **20**, 0900508 (2014).
17. Y. Chen, C. Zhao, H. Huang, S. Chen, P. Tang, Z. Wang, S. Lu, H. Zhang, S. Wen, and D. Tang, J. Lightwave Technol. **31**, 2857 (2013).
18. K. Wang, J. Wang, J. Fan, M. Lotya, A. O'Neill, D. Fox, Y. Feng, X. Zhang, B. Jiang, Q. Zhao, H. Zhang, J. N. Coleman, L. Zhang, and W. J. Blau, ACS Nano **7**, 9260 (2013).
19. S. Wang, H. Yu, H. Zhang, A. Wang, M. Zhao, Y. Chen, L. Mei, and J. Wang, Adv. Mater. **26**, 3538 (2014).
20. H. Liu, A. P. Luo, F. Z. Wang, R. Tang, M. Liu, Z. C. Luo, W. C. Xu, C. J. Zhao, and H. Zhang, Opt. Lett. **39**, 4591 (2014).
21. Z. Luo, Y. Huang, M. Zhong, Y. Li, J. Wu, B. Xu, H. Xu, Z. Cai, J. Peng, and J. Weng, J. Lightwave Technol. **32**, 4679 (2014).
22. R. I. Woodward, E. J. R. Kelleher, R. C. T. Howe, G. Hu, F. Torrisi, T. Hasan, S. V. Popov, and J. R. Taylor, Opt. Express **22**, 31113 (2014).
23. D. Mao, S. Zhang, Y. Wang, X. Gan, W. Zhang, T. Mei, Y. Wang, Y. Wang, H. Zeng, and J. Zhao, Opt. Express **23**, 27509 (2015).
24. M. Jung, J. Lee, J. Park, J. Koo, Y. M. Jhon, and J. H. Lee, Opt. Express **23**, 19996 (2015).
25. K. Wu, X. Zhang, J. Wang, X. Li, and J. Chen, Opt. Express **23**, 11453 (2015).
26. M. Zhang, G. Hu, H. Hu, R. C. T. Howe, L. Chen, Z. Zheng, and T. Hassan, Sci. Rep. **5**, 17482 (2015).
27. J. Lee, J. Park, J. Koo, Y. M. Jhon, and J. H. Lee, J. Opt. **18**, 035502 (2016).
28. R. I. Woodward, R. C. T. Howe, T. H. Runcorn, G. Hu, F. Torrisi, E. J. R. Kelleher, and T. Hasan, Opt. Express **23**, 20051 (2015).
29. B. Chen, X. Zhang, K. Wu, H. Wang, J. Wang, and J. Chen, Opt. Express **23**, 26723 (2015).
30. D. Mao, B. Du, D. Yang, S. Zhang, Y. Wang, W. Zhang, X. She, H. Cheng, H. Zeng, and J. Zhao, Small **12**, 1489 (2016).
31. J. Koo, Y. I. Jhon, J. Park, J. Lee, and Y. M. Jhon, Adv. Funct. Mater. **26**, 7454 (2016).
32. J. Lee, B.-K. Yu, Y. I. Jhon, J. Koo, S. J. Kim, Y. M. Jhon, and J. H. Lee, Adv. Opt. Mater. **5**, 1700096 (2017).
33. Y. I. Jhon, J. Koo, B. Anasori, M. Seo, J. H. Lee, Y. Gogotsi, and Y. M. Jhon, Adv. Mater., **29**, 1702496 (2017).
34. K. F. Mak and J. Shan, Nat. Photon. **10**, 216 (2016).
35. K. F. Mak, K. He, J. Shan, and T. F. Heinz, Nat. Nanotechnol. **7**, 494 (2012).
36. B. Radisavljevic, A. Radenovic, J. Brivio, V. Giacometti, and A. Kis, Nat. Nanotechnol. **6**, 147 (2011).
37. K. F. Mak, C. Lee, J. Hone, J. Shan, and T. F. Heinz, Phys. Rev. Lett. **105**, 136805 (2010).
38. Q. H. Wang, K. Kalantar-Zadeh, A. Kis, J. N. Coleman, and M. S. Strano, Nat. Nanotechnol. **7**, 699 (2012).
39. G. Zhao, S. Han, A. Wang, Y. Wu, M. Zhao, Z. Wang, and X. Hao, Adv. Funct. Mater. **25**, 5292 (2015).
40. H. Li, G. Lu, Z. Yin, Q. He, H. Li, Q. Zhang, and H. Zhang, Small **8**, 682 (2012).
41. A. Kumar and P. K. Ahluwalia, Eur. Phys. J. B **85**, 186 (2012).
42. C. Ruppert, O. B. Aslan, and T. F. Heinz, Nano Lett. **14**, 6231 (2014).
43. X.-D. Wang, Z.-C. Luo, H. Liu, M. Liu, A.-P. Luo, and W.-C. Xu, Appl. Phys. Lett. **105**, 161107 (2014).
44. J. Koo, J. Lee, W. Shin, and J. H. Lee, Opt. Mater. Express **5**, 1859 (2015).
45. Z. C. Luo, M. Liu, Z. N. Guo, X. F. Jiang, A. P. Luo, C. J. Zhao, X. F. Yu, W. C. Xu, and H. Zhang, Opt. Express **23**, 20030 (2015).
46. J. Sotor, G. Sobon, M. Kowalczyk, W. Macherzynski, P. Paletko, and K. M. Abramski, Opt. Lett. **40**, 3885 (2015).
47. K. S. Novoselov, A. K. Geim, S. V. Morozov, D. Jiang, Y. Zhang, S. V. Dubonos, I. V. Grigorieva, and A. A. Firsov, Science **306**, 666 (2004).
48. Y. M. Chang, H. Kim, J. H. Lee, and Y.-W. Song, Appl. Phys. Lett. **97**, 211102 (2010).
49. B. D. Gupta, H. Dodeja, and A. K. Tomar, Opt. Quantum Electron. **28**, 1629 (1996).
50. Y. C. Jiang, J. Gao, and L. Wang, Sci. Rep. **6**, 19624 (2016).
51. Y. Kim, Y. I. Jhon, J. Park, J. H. Kim, S. Lee, and Y. M. Jhon, Nanoscale **8**, 2309 (2016).
52. G. Cunningham, D. Hanlon, N. McEvoy, G. S. Duesberg, and J. N. Coleman, Nanoscale **7**, 198 (2015).
53. K. Wu, B. Chen, X. Zhang, S. Zhang, C. Guo, C. Li, P. Xiao, J. Wang, L. Zhou, W. Zou, and J. Chen, Opt. Commun. **406**, 214 (2017).
54. F. Wang, D. Popa, Z. Sun, T. Hasan, F. Torrisi, and A. C. Ferrari, in *Conference on Lasers and Electro-Optics 2010* (2010), paper JWA96.
55. P. Franco, M. Midrio, and A. Tozzato, J. Opt. Soc. Am. B **11**, 1090 (1994).
56. D. Popa, Z. Sun, T. Hasan, F. Torrisi, F. Wang, and A. C. Ferrari, Appl. Phys. Lett. **98**, 073106 (2011).
57. O. R. Wood and S. E. Schwarz, Appl. Phys. Lett. **11**, 88 (1967).
58. G. J. Spühler, R. Paschotta, R. Fluck, B. Braun, M. Moser, G. Zhang, E. Gini, and U. Keller, J. Opt. Soc. Am. B. **16**, 376 (1999).
59. J. Lee, J. Koo, C. Chi, and J. H. Lee, J. Opt. **16**, 085203 (2014).